Journal of Power Sources 233 (2013) 285–289

Contents lists available at SciVerse ScienceDirect

Journal of Power Sources

journal homepage: www.elsevier.com/locate/jpowsour

Short communication

Synthesis, structure, and electrochemical Li-ion intercalation of $LiRu_2O_4$ with $CaFe_2O_4$-type structure

Young Hwa Jung [a], Do Kyung Kim [a], Seung-Tae Hong [b,*]

[a] Department of Materials Science and Engineering, KAIST, Daejeon 305-701, Republic of Korea
[b] Department of Energy System Engineering, DGIST, Daegu 711-873, Republic of Korea

HIGHLIGHTS

- We synthesized for the first time the new compound $LiRu_2O_4$ with the $CaFe_2O_4$-type structure.
- The electrochemical Li intercalation of the $CaFe_2O_4$-type is reported for the first time.
- We determined Li position in the structure according to an advanced powder XRD method.
- $LiRu_2O_4$ demonstrated a reversible Li intercalation reaction at 3.2–3.5 V vs. Li/Li^+, ~80 $mAhg^{-1}$.
- Our study would promote research on other $CaFe_2O_4$-type compounds with Mn, Fe, or Ti.

GRAPHICAL ABSTRACT

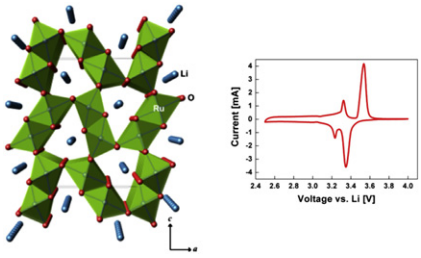

ARTICLE INFO

Article history:
Received 3 December 2012
Received in revised form
15 January 2013
Accepted 19 January 2013
Available online 29 January 2013

Keywords:
Lithium intercalation
Tunnel structure
Calcium ferrite
Lithium ruthenate
Sodium ruthenate

ABSTRACT

A new material, $LiRu_2O_4$, has been synthesized by ion-exchange reaction from $NaRu_2O_4$ that has been prepared by solid state reaction at 950 °C under Ar flow. The crystal structure of $LiRu_2O_4$, isostructural with the parent $NaRu_2O_4$, has been refined by an X-ray Rietveld method (*Pnma*, $a = 9.13940(5)$ Å, $b = 2.80070(9)$ Å, $c = 11.0017(1)$ Å, $Z = 4$, $R_p = 5.30\%$, $wR_p = 6.73\%$, $\chi^2 = 0.41$, 23 °C). The structure belongs to $CaFe_2O_4$-type, where double chains of edge-sharing octahedral RuO_6 share the corners with neighboring double chains and form tunnels in between them parallel to the shortest *b*-axis so that the one-dimensional Li array is placed inside each of the tunnels. Detailed structural analysis indicates that the tunnel inside has more than enough space to be filled with the Li atoms. The electrochemical tests of $LiRu_2O_4$ demonstrates a reversible Li intercalation reaction at 3.2–3.5 V vs. Li/Li^+ with a capacity of ~80 $mAhg^{-1}$. The material exhibits excellent high-rate characteristics (93% capacity retention at 10*C*/1*C*) as well as high capacity retention with cycles (99% at 50 cycles).

1. Introduction

Lithium intercalation materials with various crystal structures have been extensively studied [1–3] for several decades due to increasing attention for the applications as rechargeable batteries. However, the search for new electrode materials seems never-ending because recent development in electronic mobile devices and electric vehicles have brought about the need for much higher battery performances in energy and power densities, cycle life and safety than ever. Among several intercalative structure-types for lithium ion batteries, the crystal structures with one-dimensional tunnels have received attention for their easy ion diffusion and stable framework hosts [4–7].

* Corresponding author. Tel.: +82 53 785 6415; fax: +82 53 785 6409.
E-mail address: st.hong@dgist.ac.kr (S.-T. Hong).

0378-7753/$ – see front matter © 2013 Elsevier B.V. All rights reserved.
http://dx.doi.org/10.1016/j.jpowsour.2013.01.119

The calcium ferrite ($CaFe_2O_4$)-type structure, one of many different types of oxides with the same general chemical formula of AM_2O_4, is a tunnel structure [8]. Edge-sharing of MO_6 octahedra make an irregular hexagonal (or pseudo-trigonal) one-dimensional channel and A (alkali or alkaline earth metal) ions are located at the center of this channel. A number of materials with this structure show interesting magnetic and electrical properties [9–13]. Electrochemical insertion characteristics, however, have been rarely investigated. Recently, a closely-related structure has been reported for lithium ion intercalation in high pressure phase of Li_xTiO_2, an intergrowth structure between ramsdellite-type and $CaFe_2O_4$-type [14]. Here, we report synthesis, crystal structure and electrochemical properties of $LiRu_2O_4$ as not only a novel material, but also a new crystal structure-type, to the best of our knowledge, ever reported for electrochemical lithium intercalations.

2. Experimental

$NaRu_2O_4$ was first synthesized through a solid-state reaction from a mixture of Na_2CO_3 (99.5%, Aldrich) and RuO_2 (99.9%, Aldrich) with a nominal composition of Na:Ru = 1.02:2. The mixture was pressed into a pellet, and heated at 950 °C for 12 h under Ar flow. Small amount (~1%) of $Na_{3-x}Ru_4O_9$, a ruthenium bronze, was observed in the X-ray diffraction pattern as an impurity. Then, $LiRu_2O_4$ was prepared by sodium/lithium ion-exchange method in the same way as $LiMo_4O_6$ case [15]. An excess amount (0.463 g, 3.458 mmol) of LiI (beads, 99%, Aldrich) was added to $NaRu_2O_4$ powders (0.500 g, 1.729 mmol) in an Ar-filled glove box. The pellet was sealed in an evacuated fused-silica tube (a 30 cm long and 10 mm diameter), heated rapidly to 340 °C at a rate of 5 °C min^{-1} and slowly to 460 °C at a rate of 0.5 °C min^{-1}. Then, it was maintained at 460 °C for 12 h, cooled to room temperature, and washed with acetonitrile to remove remaining LiI. Less than 1% of RuO_2 and unidentified phases were observed as discernible impurities after the exchange reaction, which seemed a decomposition product from $Na_{3-x}Ru_4O_9$, in agreement with a separate ion-exchange experiment using the $Na_{3-x}Ru_4O_9$ as a major phase. The study of the decomposition reaction is beyond the scope of this work and will not be discussed.

The powder X-ray diffraction (XRD) data were collected at room temperature on a Bragg-Brentano diffractometer (Bruker D4 Endeavor) with a Cu X-ray tube (λ = 1.5418 Å) and a position-sensitive detector (LynxEye) with 3.7° slit. Data acquisition covered the angular range of $15° \le 2\theta \le 140°$ at a step width of 0.01858°. Crystal structures were confirmed and refined using the powder profile refinement program GSAS [16]. The morphology of synthesized particles was characterized using Scanning Electron Microscopy (SEM, Philips, S-4800). The chemical analysis was carried out by inductively coupled plasma-atomic emission spectroscopy (ICP-AES, Perkin Elmer, Optima 5300DV).

Electrochemical characterizations of $LiRu_2O_4$ were performed using coin-type cells consisting of cathode, polyethylene separator (Celgard), anode (Li metal) and electrolytes [1 M $LiPF_6$ in ethylene carbonate/ethyl methyl carbonate solvent (1/2, v/v)]. The electrode was fabricated by $LiRu_2O_4$, carbon black and PVdF binder in a weight ratio of 80:10:10 on an Al foil. The loading of active material was 2–3 mg cm^{-2}. All coin cells were assembled in an Ar filled glove box. Cyclic voltammetries and galvanostatic cycling tests were performed using Potentiostat VMP (Bio-Logic) and TOSCAT-3100 (Toyo), respectively.

3. Results and discussion

The XRD pattern for the synthesized $NaRu_2O_4$ (Fig. 1(a)) matched well with the previously known orthorhombic structure

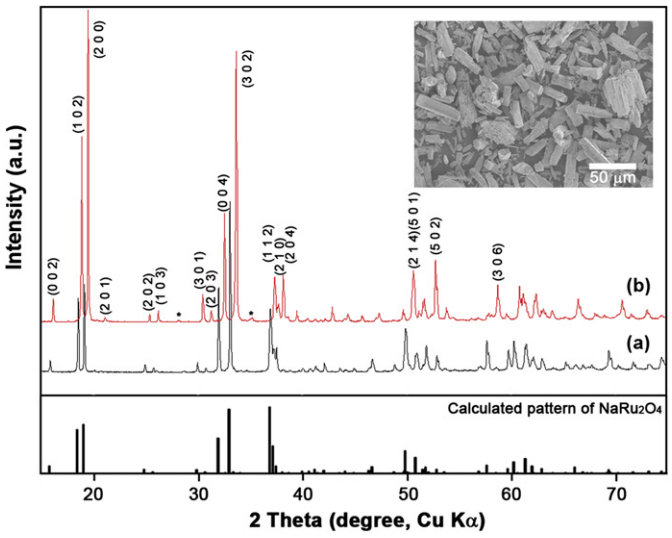

Fig. 1. X-ray diffraction patterns of (a) $NaRu_2O_4$ synthesized from solid state reaction of Na_2CO_3 and RuO_2 at 950 °C for 12 h, and (b) $LiRu_2O_4$ prepared by ion exchange reaction from $NaRu_2O_4$ at 460 °C for 12 h. * Indicates RuO_2 as an impurity phase obtained after ion exchange reaction. Inset shows a SEM image of $LiRu_2O_4$.

(space group *Pnma*, no. 62) [9], and the lattice parameters were refined as a = 9.27244(3) Å, b = 2.82080(9) Å and c = 11.1766(4) Å by the Rietveld method. It is apparent that the powder XRD pattern for $LiRu_2O_4$ is analogous to that for the Na phase as shown in Fig. 1, but all the peaks are shifted to higher angles, indicating a smaller unit cell. The same structure type was assumed, and the refined cell parameters for the Li phase are: a = 9.13940(5) Å, b = 2.80070(9) Å, and c = 11.0017(1) Å. The cell volume decreases by 3.6%, as expected from the smaller ionic size of Li^+ (0.76 Å) than Na^+ (1.02 Å) [17]. The SEM image showed that the crystals grew with a long bar-shape, presumably along the shortest b-axis, which conforms to the refined preferred orientation (P.O.) coefficients in the Rietveld refinement: the March-Dollase type P.O. coefficients of (100) and (010) are 0.584 and 2.091 with the fraction of 41.5% and 58.5%, respectively.

The amount of Li in the phase prepared by the ion-exchange was to be carefully determined because the compound is expected to have nonstoichiometric amount of lithium with the general formula $Li_{1-x}Ru_2O_4$ ($0 \le x \le 1$) like the parent Na phase [10]. The ICP analysis confirmed the absence of Na in the phase, and the Li:Ru ratio was close to 1:2, but the experimental errors were too large to confirm the precise value. Even though the possibility of lithium deficiency can not be completely excluded, the electrochemical charge/discharge characterization also indicated that the fresh electrode of $Li_{1-x}Ru_2O_4$ is equivalent to a discharged one ($x \approx 0$).

The initial structural model for $LiRu_2O_4$ was adopted from $NaRu_2O_4$ structure [9,10] for the Rietveld refinement, except the Li site. First, only ruthenium and oxygen atoms were considered and fully refined isotropically, and later the Li position was determined from the Fourier difference synthesis map in a similar way to the structure determination from the powder diffraction data described in our previous work [18]. After Rietveld fitting was carried out with a structural model only with the Ru and O atoms without Li, LeBail fitting was used to extract the structure factors which were used as input data for the single crystal refinement program, CRYSTALS [19]. Positional and isotropic thermal parameters were fully refined without the Li atoms, and then the Fourier difference map resulted in the Li coordinate. The electron density of the Li was weak as expected from its small atomic number, but clear enough to determine its location in the unit cell as presented in Fig. 2. The

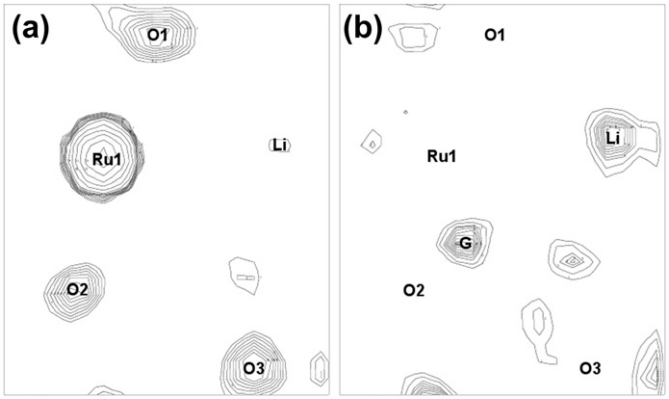

Fig. 2. (a) Observed and (b) difference Fourier maps for $LiRu_2O_4$ at $y = 0.25$. The contour levels are adjusted unequally so that weaker densities can be seen clearly.

weak but observed ghost peaks were most probably due to low data quality of powders compared to conventional single crystal data. For example, the highest ghost peak denoted as G is at a special position of (1/2, 1/4, 1/2), 1.39 Å and 1.11 Å away from Ru1 and O2, respectively. The position and the isotropic thermal parameter for the Li were fixed even in the final refinement because the X-ray refinement of such a light atom in the presence of much heavier atoms like ruthenium is not reliable at all. The final Rietveld refinement profile fits are shown in Fig. 3, and crystal data and structure refinement results are given in Table 1. The refinement parameters were scale factor, phase fractions, background, unit cell parameters, peak profile coefficients, atomic coordinates, preferred orientation coefficients [(010) and (100) directions] and isotropic displacement parameters. The refined atomic coordinate, isotropic displacement and bond valence sums [20] for $LiRu_2O_4$ are represented in Table 2. Selected metrical data for the $LiRu_2O_4$ are listed in Table 3. Bond valence sums, calculated with the program VALENCE [21] match the expected charges of the ions reasonably well. The relatively lower valence sum for O3 resulted from the longer Li–O3 interatomic distance (2.481 Å).

The refined crystal structure of $LiRu_2O_4$ is presented in Fig. 4, where the double chains of edge-sharing octahedral RuO_6 share the corners with neighboring double chains and form tunnels in

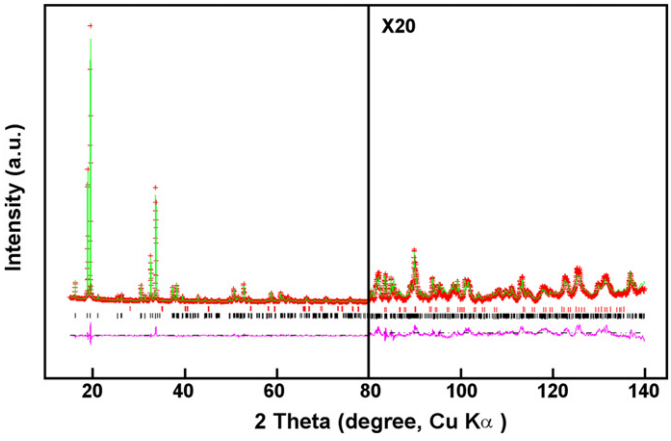

Fig. 3. X-ray Rietveld refinement profiles for $LiRu_2O_4$ including the minor impurity phase, RuO_2, recorded at room temperature. Crosses mark the observed data points (red) and the solid line is the calculated profile (green). The bottom trace shows the difference curve (purple), and the ticks denote expected peak positions for $LiRu_2O_4$ (bottom, black) and RuO_2 (top, red), respectively. (For interpretation of the references to color in this figure legend, the reader is referred to the web version of this article.)

Table 1
Crystal data and structure refinement for $LiRu_2O_4$ from powder X-ray diffraction data.

Chemical formula	$LiRu_2O_4$
Formula weight	273.08
Space group	*Pnma*, (no. 62)
Z	4
a (Å)	9.13940 (5)
b (Å)	2. 80070 (9)
c (Å)	11.0017 (1)
V (Å^3)	281.608(9)
d_{calc} (g cm^{-3})	6.441
Temperature (°C)	23
$R_p/R_{wp}/R_{exp}/R_B$ (%)	5.30/6.73/10.4/5.66
Goodness of fit (total)	0.65
Reduced χ^2	0.418
Total refined variables	29

between them parallel to the shortest *b*-axis so that the one-dimensional Li array is placed inside each of the tunnels. For the calcium ferrite-type (AM_2O_4) structure, each A site is approximately in the center position surrounded by nine oxygen atoms, where six of them consist of vertices of a trigonal prismatic polyhedron and the other three are capping the three rectangular faces of the prism. Accommodation of fractional occupancies at the A site in the tunnel is similar to the hollandite [22], another tunnel structure. It was also known that the structure has the limited radius ratio R_M/R_A in the range of 0.53–0.89 [8]. The ratios for $NaRu_2O_4$ and $LiRu_2O_4$ are 0.64 and 0.86, respectively, within the range.

The tunnel structure implies that the Li ion diffusion in this structure must be one-dimensional through the tunnels, where the distance between the neighboring Li ions is 2.80 Å, similar to 2.82 Å for $LiCoO_2$ [23], shorter than 3.00 Å for $LiFePO_4$ [24], and 3.57 Å for $LiMn_2O_4$ [25]. It should be also noted that the tunnel inside has more space than that needed to just fit with the lithium atoms. For the Na phase, the inside volume seems to just fit: The Na atom is around in the center position of the trigonal prismatic polyhedron, and the Na–O distances [9] are 2 × 2.37 Å, 2 × 2.39 Å and 2 × 2.48 Å, with an average of 2.41 Å which matches well with the expected Na–O distance of 2.42 Å from the ionic radii sum [17]. The three capping oxygen atoms are distant at 2.55, 2.56 and 3.61 Å, respectively. On the other hand, if Li atom for the Li phase is located in the center position of the polyhedron, the average Li–O distance would be 2.30 Å, shorter than 2.41 Å due to smaller unit cell, but too long for the expected Li–O distance of 2.16 Å [17]. This implies that the tunnel has more than enough space to be filled with the Li atoms. In fact, according to the Fourier maps the Li position was observed to be shifted so that two oxygen atoms are relatively closer (2.05 Å) than the other four (2.33 or 2.48 Å), keeping the average distance of 2.30 Å. One of the face-capping oxygen comes significantly closer to 2.26 Å, while the other two capping oxygen atoms are distant at 3.01 or 3.58 Å, respectively.

Table 2
Atomic coordinates, isotropic displacement (Å^2), and bond valence sums (v.u.) for $LiRu_2O_4$ at room temperature.

Atom	Wyckoff	*x*	*y*	*z*	U_{iso}*100	BVS
Li1	4*c*	0.725	1/4	0.642	1.25	0.87
Ru1	4*c*	0.44539(12)	1/4	0.61818(12)	1.17(3)	3.55
Ru2	4*c*	0.41052(11)	1/4	0.10191(11)	1.17(3)	3.46
O1	4*c*	0.5395(7)	1/4	0.7773(8)	2.4(2)	2.20
O2	4*c*	0.4041(8)	1/4	0.4417(7)	2.4(2)	2.15
O3	4*c*	0.2006(8)	1/4	0.1824(6)	2.4(2)	1.69
O4	4*c*	0.6237(8)	1/4	0.0292(8)	2.4(2)	1.84

Table 3
Selected interatomic distances (Å) in $LiRu_2O_4$ at room temperature.

Li1–Li1	2.8007 (1)	Ru1–O2	2 × 2.071 (6)
Li1–O1	2.256 (8)	Ru1–O3	2 × 2.060 (5)
Li1–O2	2 × 2.050 (5)	Ru2–O1	2 × 1.984 (6)
Li1–O3	2.481 (6)	Ru2–O3	2.113 (7)
Li1–O4	2 × 2.326 (6)	Ru2–O4	2.106 (8)
Ru1–O1	1.951 (9)	Ru2–O4	2 × 2.035 (6)
Ru1–O2	1.977 (7)	–	–

Fig. 5 shows a cyclic voltammogram of an electrode of $LiRu_2O_4$ in the range from 2.5 to 4.0 V with the scanning rate of 0.5 mV s^{-1} at room temperature. There appeared two reduction peaks at 3.35 and 3.23 V, and the corresponding oxidation peaks at 3.53 and 3.32 V, respectively, showing a reversible Li intercalation reaction. The galvanostatic charge/discharge profiles are shown in Fig. 6(a). Two discharge plateaus were observed at around 3.4 and 3.3 V, consistent with the cyclic voltammogram result. The initial discharge capacity at a current rate of *C*/10 is about 80 $mAhg^{-1}$ whereas the theoretical one is 98 $mAhg^{-1}$ per 1 Li (In this work, 1*C* corresponds to 80 mAg^{-1}). The gravimetric capacity is relatively low compared to those for the 3*d* transition metal oxide materials due to containing heavy Ru atom. However, it is interesting to note the superior behavior at higher rates up to 10*C* as shown in Fig. 6(a): 93% of capacity retention at the 10*C*-rate over 1*C*-rate. It is well known that particle size effects become very important for compounds with one-dimensional diffusion like $LiFePO_4$, as shown by the excellent higher rate performance for the nano-sized $LiFePO_4$ compared to a micro-sized one [26]. It is to be noted that $LiRu_2O_4$ synthesized for the present experiment consists of tens of micro-sized particles but still exhibits excellent high-rate characteristics. Such a result might be from weak Li ion diffusion barriers due to the distinctive crystal structure with the wide space inside the tunnels and the short Li–Li diffusion length (2.80 Å). In addition, it exhibits fairly high capacity retention with cycles, suggesting high structural stability during Li de/insertion: the discharge capacity was about

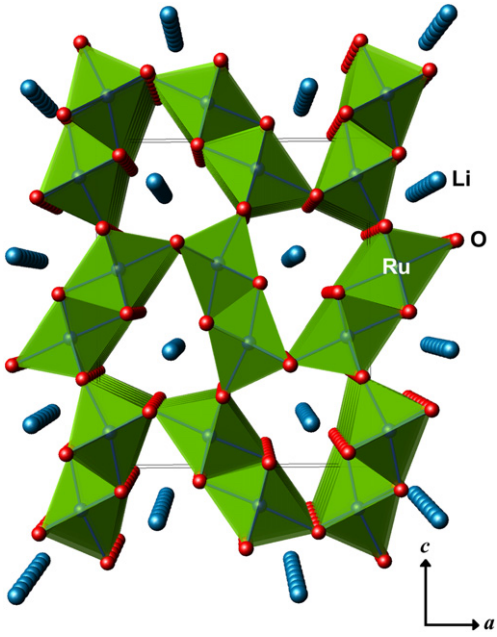

Fig. 4. (010) view of the crystal structure of $LiRu_2O_4$. RuO_6 and Li are shown as octahedra (green in the electronic version of paper) and spheres (blue), respectively. The unit cell is outlined. (For interpretation of the references to color in this figure legend, the reader is referred to the web version of this article.)

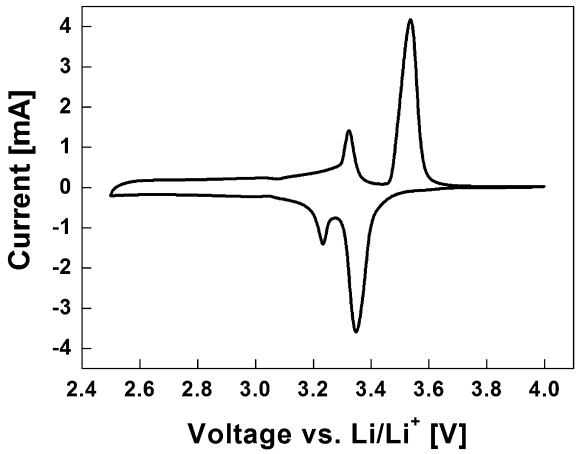

Fig. 5. Cyclic voltammogram of $LiRu_2O_4$ (scan rate = 0.5 mV s^{-1}).

99% of the initial one even after 50 cycles of charge/discharge at a current rate of *C*/2 as shown in Fig. 6(b). It is noteworthy to compare with the very poor cycleability of α-MnO_2, a hollandite-type structure with much bigger tunnels. It seems that too big a tunnel is not stable upon intercalation reaction. When the tunnels of α-MnO_2 are occupied by other molecules or cations such as Li_2O, NH^{4+}, Rb^+ or K^+, a better cycle performance was observed due to structure stability [27].

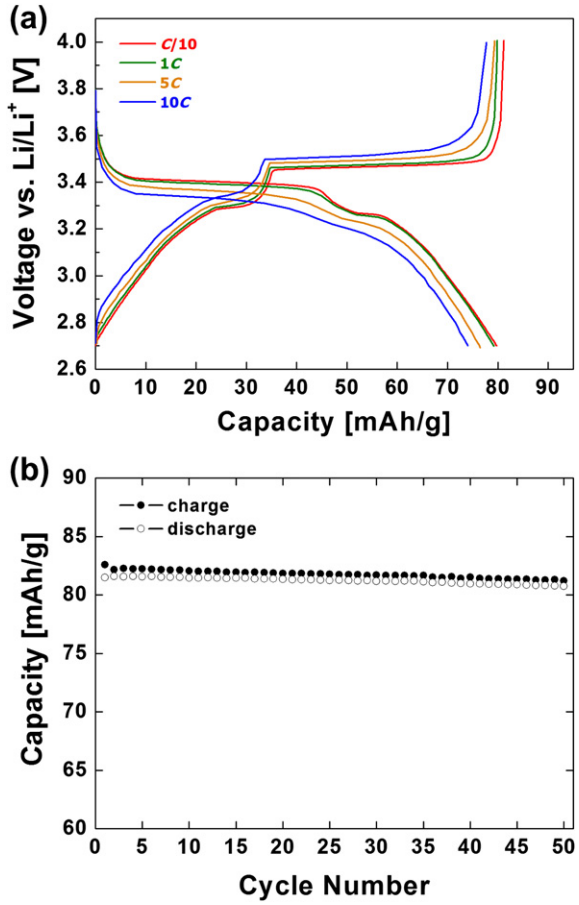

Fig. 6. (a) Charge/discharge voltage profiles for $LiRu_2O_4$ at 25 °C and various *C*-rates, and (b) cycling performance for $LiRu_2O_4$ at 25 °C and *C*/2-rate between 2.7 and 4.0 V.

4. Conclusions

In the present study we report the synthesis and crystal structure of a new compound, $LiRu_2O_4$ with the $CaFe_2O_4$-type structure. In the crystal structure of $LiRu_2O_4$, double chains of edge-sharing octahedral RuO_6 share the corners with neighboring double chains and form tunnels in between them parallel to the shortest *b*-axis so that the one-dimensional Li array is placed inside each of the tunnels. The tunnel inside has more than enough space to be filled with the Li atoms. $LiRu_2O_4$ demonstrated a reversible Li intercalation reaction at 3.2–3.5 V vs. Li/Li^+ with a capacity of ~80 $mAhg^{-1}$, exhibiting excellent high-rate characteristics as well as high capacity retention with cycles. The electrochemical lithium intercalation of the calcium ferrite type compound has been characterized for the first time. This work would provide an important basis for understanding the structure–property relationship as well as promoting a further investigation of new materials of the structure type by substitution of ruthenium with other transition metals like Mn, Fe, Ti or else.

Acknowledgments

This work was supported by the DGIST R&D Program of the Ministry of Education, Science and Technology of Korea (12-BD-0405). It was also supported by Program to Solve Climate Changes (NRF-2010-C1AAA001-2010-0029031) through the National Research Foundation of Korea (NRF) funded by the Ministry of Education, Science and Technology.

References

[1] M.S. Whittingham, Chem. Rev. 104 (2004) 4271–4302.
[2] T. Ohzuku, R.J. Brodd, J. Power Sources 174 (2007) 449–456.
[3] B.L. Ellis, K.T. Lee, L.F. Nazar, Chem. Mater. 22 (2010) 691–714.
[4] A.K. Padhi, K.S. Nanjundaswamy, J.B. Goodenough, J. Electrochem. Soc. 144 (1997) 1188–1193.
[5] M.M. Thackeray, Prog. Solid State Chem. 25 (1997) 1–71.
[6] L.D. Noailles, C.S. Johnson, J.T. Vaughey, M.M. Thackeray, J. Power Sources 81-82 (1999) 259–263.
[7] N. Sharma, J. Plevert, G.V.S. Rao, B.V.R. Chowdari, T.J. White, Chem. Mater. 17 (2005) 4700–4710.
[8] Hk. Müller-Buschbaum, J. Alloys Compd. 349 (2003) 49–104.
[9] K.A. Regan, Q. Huang, M. Lee, A.P. Ramirez, R.J. Cava, J. Solid State Chem. 179 (2006) 195–204.
[10] R.V. Panin, N.R. Khasanova, A.M. Abakumov, W. Schnelle, J. Hadermann, E.V. Antipov, Russ. Chem. Bull. Int. Ed. 55 (2006) 1717–1722.
[11] S. Zouari, L. Ranno, A. Cheikh-Rouhou, O. Isnard, P. Wolfers, P. Bordet, P. Strobel, J. Alloys Compd. 452 (2008) 234–240.
[12] K. Yamaura, Q. Huang, L. Zhang, K. Takada, Y. Baba, T. Nagai, Y. Matsui, K. Kosuda, E. Takayama-Muromachi, J. Am. Chem. Soc. 128 (2006) 9448–9456.
[13] H. Mizoguchi, L.N. Zakharov, A.P. Ramirez, W.J. Marshall, A.W. Sleight, M.A. Subramanian, Inorg. Chem. 48 (2009) 204–208.
[14] M. Mamiya, K. Kataoka, S. Kikuchi, Y. Terajima, K. Tokiwa, J. Akimoto, J. Phys. Chem. Solids 73 (2012) 1460–1462.
[15] R.L. Gitzendanner, F.J. DiSalvo, J. Alloys Compd. 218 (1995) 9–12.
[16] A.C. Larson, R.B. Von Dreele, GSAS; Report LAUR 86–748, Los Alamos National Laboratory, New Mexico, USA, 2000.
[17] R.D. Shannon, Acta Crystallogr. A32 (1976) 751–767.
[18] E. Lee, S.-T. Hong, J. Solid State Chem. 181 (2008) 2930–2934.
[19] P.W. Betteridge, J.R. Carruthers, R.I. Cooper, K. Prout, D.J. Watkin, J. Appl. Crystallogr. 36 (2003) 1487.
[20] I.D. Brown, D. Altermatt, Acta Crystallogr. B41 (1985) 244–247.
[21] C. Hormillosa, S. Healy, T. Stephen, I.D. Brown, Bond Valence Calculator, Version 2.0, McMaster University, Canada, 1993.
[22] C.M. Plug, J. Solid State Chem. 41 (1982) 23–26.
[23] W.D. Johnston, R.R. Heikes, D.E. Sestrich, J. Phys. Chem. Solids 7 (1958) 1–13.
[24] V.A. Strel'tsov, E.L. Belokoneva, V.G. Tsirel'son, N.K. Hansen, Acta Crystallogr. B49 (1993) 147–153.
[25] A. Mosbah, A. Verbaere, M. Tournoux, Mat. Res. Bull. 18 (1983) 1375–1381.
[26] R. Malik, D. Burch, M. Bazant, G. Ceder, Nano Lett. 10 (2010) 4123–4127.
[27] C.S. Johnson, D.W. Dees, M.F. Mansuetto, M.M. Thackeray, D.R. Vissers, D. Argyriou, C.-K. Loong, L. Christensen, J. Power Sources 68 (1997) 570–577.